

# A Method to Determine the Strain and Nucleation Sites of Stacked Nano-Objects

Sergio I. Molina<sup>1,2,\*</sup>, María Varela<sup>1</sup>, Teresa Ben<sup>2</sup>, David L. Sales<sup>2</sup>, Joaquín Pizarro<sup>3</sup>, Pedro L. Galindo<sup>3</sup>, David Fuster<sup>4</sup>, Yolanda González<sup>4</sup>, Luisa González<sup>4</sup>, and Stephen J. Pennycook<sup>1</sup>

<sup>1</sup>Materials Science and Technology Division, Oak Ridge National Laboratory, Oak Ridge TN 37831, USA

<sup>2</sup>Departamento de Ciencia de los Materiales e I.M. y Q.I., Facultad de Ciencias, Universidad de Cadiz, Campus Río San Pedro, s/n, 11510 Puerto Real, Cadiz, Spain

<sup>3</sup>Departamento de Lenguajes y Sistemas Informáticos, CASEM, Universidad de Cádiz, Campus Río San Pedro, s/n, 11510 Puerto Real, Cádiz, Spain

<sup>4</sup>Instituto de Microelectrónica de Madrid (CNM, CSIC), Isaac Newton 8, 28760 Tres Cantos, Madrid, Spain

Delivered by Ingenta to:

We determine the compositional distribution with atomic column resolution in a horizontal nanowire from the analysis of aberration-corrected high resolution Z-contrast images. The strain field in a layer capping the analysed nanowire is determined by anisotropic elastic theory from the resulting compositional map. The reported method allows preferential nucleation sites for epitaxial nanowires to be predicted with high spatial resolution, as required for accurate tuning of desired optical properties. The application of this method has been exemplified in this work for stacked InAs(P) horizontal nanowires grown on InP separated by 3 nm thick InP layers, but we propose it as a general method to be applied to other stacked nano-objects.

**Keywords:** Nanowire, Nano-Object, Semiconductor Nanostructure, Strain, High Resolution Z-Contrast Imaging.

## 1. INTRODUCTION

The growth of self-assembled semiconductor quantum dots was published for the first time in 1985.<sup>1</sup> These nano-objects are formed when several monolayers were epitaxially deposited on a lattice-mismatched substrate, through a transition 2D to 3D growth via a Stranski-Krastanov process. This transition is induced by the elastic strain accumulated in the 2D epitaxial layer. Following similar approaches, other semiconductor nano-objects have been produced, such as quantum wires and nano-rings. Since then, a huge effort has been dedicated to investigate the mechanisms of formation of these nano-objects. This is justified because since their discovery the confinement of charge carriers in 0D (nanodots) or 1D (nanowires) has opened the doors to achieving new optoelectronic properties.

Strain-driven processes at the nanoscale have been demonstrated to be a critical factor in the formation of self-assembled semiconductor nano-objects. In fact, the driving force for their formation has been proven to be the strain in most cases studied.<sup>2</sup> Strain associated with these

nanostructures has been measured or modelled by several approaches,<sup>3–7</sup> although finite element (FE) method has been proven to be one of the most efficient procedures.<sup>8–11</sup> The application of FE analysis to solve isotropic and anisotropic elastic theory equations to determine the strain in and around semiconductor nano-objects has been done in many cases assuming a certain simplified model that represent the studied nano-object.

The growth temperature for layers capping stacked nanowires is a critical parameter that permits the control of the heterogeneous strain field associated to the buried nanowires and hence the location of the preferential sites for the nucleation of the subsequent stacked nanowires. This is due to the influence of this temperature on the size<sup>12</sup> and probably in the compositional distribution of the grown wires. For low capping temperature (380 °C), nanowires are randomly distributed for 20 nm thick capping layers. On the other hand, for 5 nm thick capping layers, they are well ordered, and arranged along a direction that forms 9° with the [001] vertical direction. This ordered distribution of stacked nanowires was explained in a previous work<sup>13</sup> by determining the strain field at the surface of the capping layer from compositional maps obtained by electron energy loss spectrum images. A thinner capping

\*Author to whom correspondence should be addressed.

layer thickness is needed to orderly arrange the stacked wires if the growth temperature of the capping layer is higher. This is due to the reduced size of the nanowires grown with high temperature capping layers that generate weaker strain fields.

In this work, we present a method to measure by FE analysis the strain in a capped nano-object. The method consists of determining the composition in the nano-object with atomic column spatial resolution from aberration-corrected high resolution Z-contrast images. Once the compositional distribution in the nano-object is determined, we calculate the strain by solving the anisotropic elastic theory equations. We exemplify here the application of this method to InAs(P) horizontal nanowires grown on InP separated by 3 nm thick InP layers. The application of the method to this case quantitatively explains the experimentally observed distribution of the grown stacked nanowires.

## 2. EXPERIMENTAL DETAILS

For this work, two samples (A and B) of InAs(P) nanowires were grown by solid-source molecular beam epitaxy (MBE) on an InP (001) substrate by depositing InAs at 0.1 monolayers per second (ML/s) at a substrate temperature  $T_s = 515$  °C and As<sub>4</sub> beam equivalent pressure of  $2.3 \times 10^{-6}$  mbar. The amount of InAs deposited corresponded to the critical thickness for wire formation.<sup>14</sup> The grown wires are oriented along  $[1\bar{1}0]$  and periodically arranged along  $[110]$ . In the first sample (A), after wire formation, a cap layer of 20 nm of InP was grown at 515 °C by MBE at 1 ML/s. Sample B consists of seven stacked layers of nanowires separated by 3 nm thick InP spacer layers grown under the same conditions as sample A. The last layer of nanowires is uncapped.

Electron-transparent specimens for scanning transmission electron microscopy (STEM) were produced by mechanical thinning and ion milling. Milling conditions were carefully controlled to minimize the material degradation and contamination. Aberration-corrected Z-contrast images were taken at 100 kV using a dedicated VG Microscopes HB501UX STEM with a Nion aberration corrector. The third and fifth order spherical aberration coefficients are  $-50$   $\mu\text{m}$  and  $63$  mm, respectively, the inner detector angle is 64 mrad and the objective aperture angle is 27 mrad.

## 3. RESULTS AND DISCUSSION

Figure 1(a) shows a high resolution Z-contrast image of a nanowire of sample A. A low magnification Z-contrast image of stacked nanowires in sample B is presented in Figure 1(b). This image shows that the stacked nanowires of the second and upper layers are ordered with respect to the nanowires of the first layer. The ordered distribution of

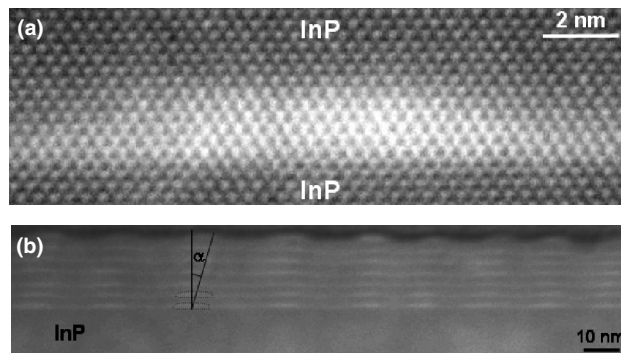


**Fig. 1.** (a) High-resolution cross-sectional aberration-corrected Z-contrast image of a nanowire in sample A. (b) Low magnification Z-contrast image of stacked nanowires in sample B. Angle  $\alpha$  is shown on this image. Brighter regions of both images correspond to InAs<sub>x</sub>P<sub>1-x</sub>.

the nanowires of the second layer is due to the influence of the heterogeneous strain field generated by the nanowires of the first layer. The strain field generated by the buried nanowires in the respective InP capping layers favours the nucleation of stacked wires along a direction close to  $[001]$ . The nanowire is formed by a disordered InAs<sub>x</sub>P<sub>1-x</sub> alloy. This material has the sphalerite crystalline structure. The  $[110]$  projection of this structure consists of atomic dumbbells arranged in centred rectangles (see Fig. 2(a)). Each dumbbell comprises two atomic columns, one containing only In atoms throughout the whole material while each neighbouring atomic column is either pure As or contains a distribution of As and P atoms, which we assume is random in thickness based on the one dimensional nature of the wire.

The intensity of Z-contrast images is strongly dependent on the atomic number of the elements that constitute each probed atomic column.<sup>15</sup> We have quantified, in the Z-contrast image of Figure 1(a), the integrated intensities around each dumbbell as illustrated in Figure 2(a). By integrating the intensity we avoid the need to exactly match the dumbbell contrast, which depends sensitively on microscope parameters such as defocus and specimen parameters such as orientation. Figure 2(b) shows the distribution of integrated intensities superimposed over the original Z contrast image. Higher values of these integrated intensities correspond to higher average Z numbers associated with the atomic columns of the dumbbells. In our case, higher intensities mean higher As content. All the intensities have been integrated from the black level subtracted raw Z contrast image without any noise reduction. Low pass filtered Z contrast images were used only to locate the position of intensity maxima associated with the In atomic columns. Figure 2(c) shows a map of the measured integrated intensities after normalization (by assigning 0 to the minimum and 1 to the maximum intensity) and interpolation. Maximum intensity of this map is clearly located on the right inner part of the nanowire.

The study of similar nanowires by grazing-incidence diffraction anomalous fine structure (GIDAFS) concluded

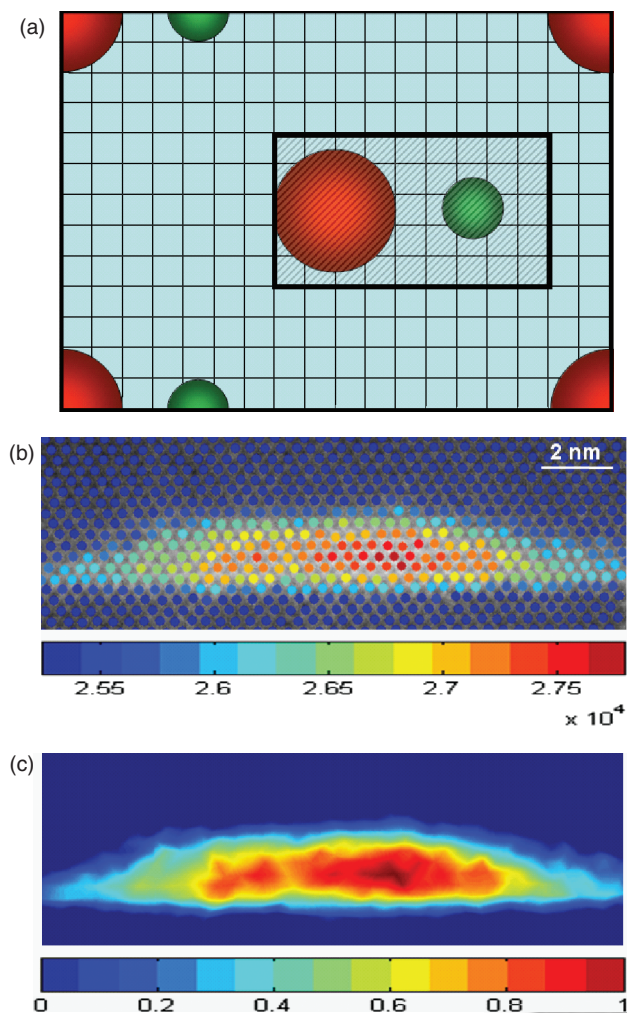


**Fig. 2.** (a) The rectangular area where intensities of Z-contrast images have been integrated is represented on the  $\langle 110 \rangle$  projection of the spherulite structure. In our case, the red colour atoms correspond to In and the green colour atoms to P and/or As atomic columns. (b) Areal integrated intensities for each atomic dumbbell are shown overlapped on the original Z-contrast image of Figure 1(a). (c) Interpolated normalized intensities from integrated intensities shown in (b). Intensities are normalized assigning 0 to the minimum and 1 to the maximum intensity.

that part of the core of these wires is made essentially of InAs.<sup>16</sup> This result is in good agreement with the compositional analysis of spatially resolved electron energy loss spectra from the inner regions of the core with the maximum Z-contrast image intensity. Taking into account these facts, we assign a composition of 100% InAs to the maximum intensity of the Z-contrast STEM images of the analyzed wires. On the other hand, substrate and capping layers are comprised of pure InP. Therefore, there are two integrated intensity values for which the As composition has been assigned, one corresponds to pure InAs and another to pure InP.

There are two issues that complicate a direct mapping of composition assuming a linear variation of intensity with composition between these two limiting values. Increasing

the average Z of a column will increase the tendency of the probe to be channelled along the column. This has the effect of increasing the amount of high angle scattering due to interaction of the probe intensity with the thermal diffuse scattering (TDS) potential. While initially leading to an increase in the detected Z-contrast signal, there is also significant attenuation of the elastic wave function of the probe due to absorption. The intensity of the probe is hence reduced leading to a reduction in the Z-contrast signal as the probe propagates through the sample. We therefore performed dynamical simulations for the whole range of As compositions, from 0 to 1, using the specimen thickness (33 nm) of the analysed region. This thickness has been measured from the ratio of the plasmon peak to the zero-loss peak of an electron energy loss spectra image of that region, as described in Ref. [17]. These simulations are performed by calculating the intensity from the absorptive potential corresponding to high-angle TDS and the wave function equivalent to the propagating probe within the sample<sup>18</sup> for the Z-contrast imaging conditions used. Integrated simulated intensities, as defined in Figure 2(a), are shown in Figure 3. It is seen that the intensities deviate only slightly from a linear dependence on composition, and for simplicity we take a linear fit as an initial model. We will find this is sufficient to predict the experimental growth behavior. The second issue concerns the well-known problem that simulated images predict higher contrast than experimental images, i.e., there is a background on experimental images whose origin at this time has not been established.<sup>19</sup> We therefore assume for now that this factor is also linear with composition, and we directly interpolate experimental integrated intensities for intermediate  $\text{InAs}_x\text{P}_{1-x}$  compositions between InP and InAs from the measured intensities of the two pure materials. Figure 2(c) can therefore be directly interpreted as an As compositional map obtained for each dumbbell of the analysed nanowire.

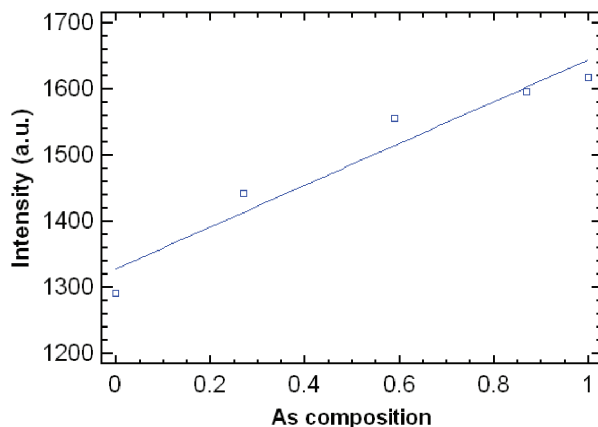


**Fig. 3.** Simulated intensities (integrated as defined in Fig. 2(a)) versus the As composition. The represented straight line is fitted by the least squares method.

The strain field is then obtained from the compositional map by solving the equations of the anisotropic elastic theory by finite element methods.<sup>13</sup> Figure 4 shows the [110] component of the strain, that is, along the direction perpendicular to the analysed nanowire, on the surface of a 3 nm InP capping layer. As we discussed in a previous article,<sup>13</sup> the maximum value of this strain component corresponds to the surface location where InAs will grow with minimum strain, and therefore it will decide the location of the preferential sites for nucleation of nanowires in the subsequent stacked layer. The nanowires of sample B (see Fig. 1(b)) are stacked along a direction that forms a small angle with the vertical [001]. The value of  $\alpha$  angle, as shown in Figure 1(b), quantifies the displacement of the nucleation sites of the nanowires of the second layer with respect to the lower nanowires of the first layer. The experimental value of this angle is  $16 \pm 8^\circ$  for the nanowires

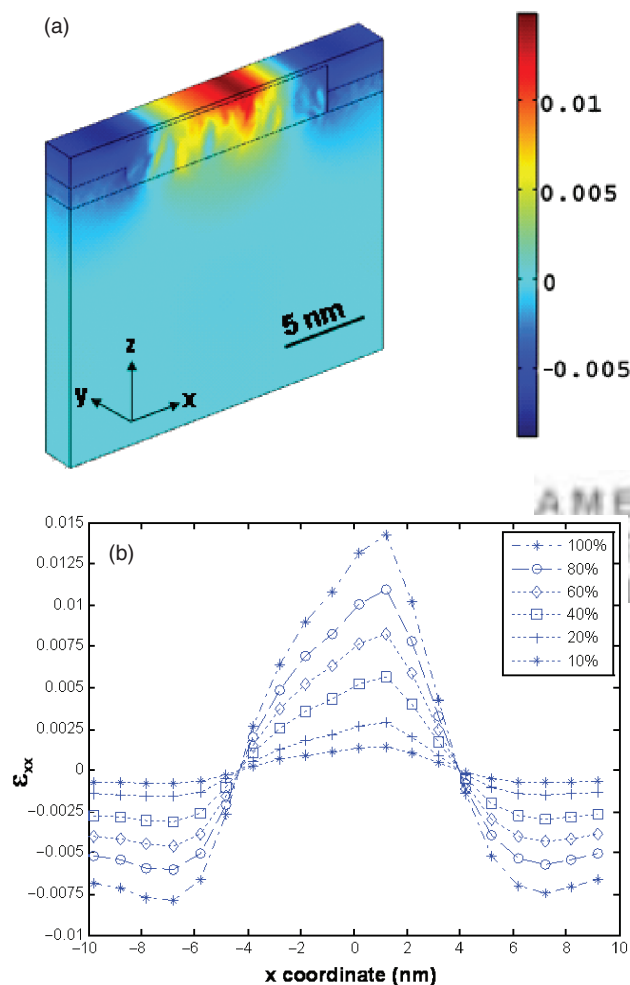


**Fig. 4.** (a) 3D representation of the [110] strain component along [110] ( $\epsilon_{xx}$ ) determined by finite element analysis from the compositional map of Figure 3(b). (b) Profile of  $\epsilon_{xx}$  along [110] across the nanowire at the growth surface of a 3 nm thick InP capping layer assigning different compositions to the maximum integrated intensity ( $\text{InAs}_x\text{P}_{1-x}$   $10\% < x < 100\%$ ). Note that the maximum strain is displaced 0.9 nm from the nanowire centre for all the cases.  $x = [110]$ ;  $y = [110]$ ;  $z = [001]$ .

of sample B. The  $\alpha$  angle determined by finite element calculations from the obtained compositional map is  $16.7^\circ$ . Therefore there is a good agreement between the experimental  $\alpha$  angle and the angle determined from the analysis of high resolution aberration-corrected Z-contrast images.

The main error of the obtained compositional map is likely to be the composition assigned to the maximum integrated intensity. We have repeated the whole process assigning other compositions (with an As content below 100%) to the maximum integrated intensity in the Z-contrast image of Figure 2(b). Strain fields have been calculated assigning As percentages of 10, 20, 40, 60, 80 and 100% to the maximum integrated intensity and the corresponding results are represented in Figure 4(b). The key point is that the maximum strain for each composition below 100% has a smaller value, but its *location* does not change. Therefore, the prediction of the alpha angle is valid even if the composition that corresponds to the maximum areal integrated intensity were smaller. Other possible sources of error are (i) the procedure that we have used to correct the effect of the background signal in the experimental images, that has been assumed to be linear with the As composition, and (ii) the existence of small local specimen thickness fluctuations and surface damage due to the ion milling process, and (iii) neglecting the non-linearity in the dependence of intensity on composition. Further work is under development to increase the accuracy of the approach proposed in this letter to determine the compositional mapping from high resolution aberration-corrected Z-contrast images with atomic column spatial resolution. However, the approach presented in this work has allowed us to estimate the compositional distribution column by column in a nanowire with sufficient accuracy to quantify the stacking angle of stacked nanowires.

#### 4. CONCLUSION

In conclusion, a method has been developed to determine with atomic column spatial resolution the compositional distribution of nanomaterials from aberration-corrected Z-contrast images. The obtained compositional distribution has been applied to determine the strain field generated by a buried nanowire. This field has been calculated by solving the equations of the anisotropic elastic theory by finite element analysis. As a demonstration of the usefulness of this approach, the location of the preferential sites for the epitaxial growth of stacked nanowires has successfully been explained from the determined strain field.

**Acknowledgment:** The authors gratefully acknowledge the comments of Dr. M. P. Oxley. This work was supported by the DOE Office of Basic Energy Sciences, Division of Materials Sciences and Engineering, the SANDiE European Network of Excellence (Contract No NMP4-CT-2004-500101), the Spanish MEC (TEC2005-05781-C03-01 y 02, NAN2004-09109-C04-01, Consolider-Ingenio

2010 CSD2006-00019), the CAM (S 0505ESP 0200) and the Junta de Andalucía (PAI research groups TEP-120 and TIC-145; project PAI05-TEP-00383).

## References and Notes

1. L. Goldstein, F. Glas, J. Y. Marzin, M. N. Charasse, and G. Le Rous, *Appl. Phys. Lett.* 47, 1099 (1985).
2. V. A. Shchukin and D. Bimberg, *Rev. Mod. Phys.* 71, 1125 (1999).
3. F. Glas, *Appl. Surf. Sci.* 188, 9 (2002).
4. E. Pan, F. Han, and J. D. Albrecht, *J. Appl. Phys.* 98, 13534 (2005).
5. D. A. Faux and U. M. E. Christmas, *J. Appl. Phys.* 98, 33534 (2005).
6. V. A. Shchukin, D. Bimberg, T. P. Munt, and D. E. Jesson, *Phys. Rev. B* 70, 85416 (2004).
7. G. Russo and P. Smereka, *J. Comput. Phys.* 214, 809 (2006).
8. Y. W. Zhang, S. J. Xu, and C.-H. Chiu, *Appl. Phys. Lett.* 74, 1809 (1999).
9. G. R. Liu and S. S. Q. Jerry, *Semicond. Sci. Technol.* 17, 630 (2002).
10. P. Liu, Y. W. Zhang, and C. Lu, *Phys. Rev. B* 68, 195314 (2003).
11. Q. X. Pei, C. Lu, and Y. Y. Wang, *J. Appl. Phys.* 93, 1487 (2003).
12. D. Fuster, M. U. Gonzalez, L. Gonzalez, Y. Gonzalez, T. Ben, A. Ponce, S. I. Molina, and J. Martinez-Pastor, *Appl. Phys. Lett.* 85, 1424 (2004).
13. S. I. Molina, T. Ben, D. L. Sales, J. Pizarro, P. L. Galindo, M. Varela, S. J. Pennycook, D. Fuster, Y. González, and L. González, *Nanotechnology* 17, 5652 (2006).
14. D. Fuster, J. Martínez-Pastor, L. González, and Y. González, *J. Phys. D* 39, 4940 (2006).
15. M. Varela, A. R. Lupini, K. van Benthem, A. Y. Borisevich, M. F. Chisholm, N. Shibata, E. Abe, and S. J. Pennycook, *Annu. Rev. Mater. Res.* 35, 539 (2005).
16. S. Grenier, M. G. Proietti, H. Renevier, L. Gonzalez, J. M. Garcia, and J. Garcia, *Europhys. Lett.* 57, 499 (2002).
17. R. F. Egerton, *Electron Energy-Loss Spectroscopy in the Electron Microscope*, Plenum, New York (1986).
18. K. A. Izhizuka, *Ultramicroscopy* 90, 71 (2002).
19. D. O. Klenov and S. Stemmer, *Ultramicroscopy* 106, 889 (2006).

Received: 2 May 2007. Accepted: 10 August 2007.

Delivered by Ingenta to:  
Oak Ridge National Laboratory  
IP : 160.91.159.246  
Mon, 23 Feb 2009 16:12:59

